Desalination and Water Treatment
www.deswater.com
doi: 10.1080/19443994.2015.1048737

57 (2016) 12168–12177
June

Taylor & Francis
Taylor & Francis Group

Synthesis and characterization of polyaniline/Zr-Co-substituted nickel ferrite ($NiFe_{1.2}Zr_{0.4}Co_{0.4}O_4$) nanocomposites: their application for the photodegradation of methylene blue

Muhammad Aamir[a], Muhammad Naeem Ashiq[a,*], Ghazala Yasmeen[a], Bashir Ahmad[a], Muhammad Fahad Ehsan[b,1], Tao He[b]

[a]*Institute of Chemical Sciences, Bahauddin Zakariya University, Multan 60800, Pakistan, Tel. +92 3006372302; email: aamirmirza321@yahoo.com (M. Aamir), Tel. +92 300 9879344; emails: naeemashiqqau@yahoo.com, naeembzu@bzu.edu.com (M.N. Ashiq), Tel. +92 3006345628; email: ghazala31pk@yahoo.com (G. Yasmeen), Tel. +92 3457356064; email: ahmadbashir_87@yahoo.com (B. Ahmad)*

[b]*National Center for Nanoscience and Technology, Beijing, R.P. China, Tel. +86 18810535912; email: m.fahad.ehsan@gmail.com (M.F. Ehsan), Tel. +86 1082545655; email: het@nanoctr.cn (T. He)*

Received 25 September 2014; Accepted 29 April 2015

ABSTRACT

In the present work, different composites of polyaniline (PANI) with various contents of Zr-Co-substituted nickel ferrite with formula ($NiFe_{1.2}Zr_{0.4}Co_{0.4}O_4$) (12.5, 25, 37.5, and 50% w/w) nanoparticles (NPs) were synthesized. These composites were characterized by X-ray diffraction (XRD), UV/Visible, Brunauer–Emmett–Teller (BET), X-ray photoelectron spectrometer (XPS), and scanning electron microscopy (SEM) analysis, and are used for the photodegradation of methylene blue (MB) from aqueous media. Effects of reaction time, NPs concentration, and degradation kinetics studies have been investigated. The structure of nickel ferrite was confirmed by XRD analysis while surface area, pore size, and morphology were investigated by BET and SEM analyses. The elements oxidation states were confirmed by XPS analysis while the optical studies were investigated by UV/Visible analysis. The degradation rate was observed fast at initial stages and then became slow. The degradation of MB follows the first-order kinetic. The NPs amount present in the composite shows remarkable influence on the degradation efficiency and is increased with the increase in nickel ferrite contents. The maximum degradation of MB was found to be 97% for the PANI/NPs composite containing 50% w/w NPs. The percentage degradation in the present work is much higher as compared to other photocatalysts reported earlier in the literature.

Keywords: Photocatalyst; Methylene blue; Zr-Co-substituted nickel ferrite; PANI composite

1. Introduction

In the recent years, nanomaterials like metals (gold, silver), carbon, and polymers (especially conducting polymers) have received great attention because of their unique optical, electronic, chemical, and mechanical properties [1]. Conducting polymers such as polyaniline (PANI) have generated much interest in scientific research as suitable candidates for the

*Corresponding author.

[1]Institute of Chemical Sciences, Bahauddin Zakariya University, Multan 60800, Pakistan.

replacement of metals. Among the various conducting polymers, PANI has a special representation due to its easy synthesis, environmental stability, low cost, and high conductivity [2]. PANI exhibits dramatic changes in its electronic structure and physical properties at protonated state. Depending on the oxidation level, PANI can be synthesized in various insulating forms such as the fully reduced leucoemeraldine base (LEB), half-oxidized emeraldine base (PANI-EB), and fully oxidized pernigraniline base (PNB). Among these three forms, PANI-EB is the most stable and widely investigated polymer in this family. PANI-EB differs substantially from LEB and PNB in the sense that its conductivity can be tuned via doping from 10^{-10} to 100 s/cm and more, whereas the LEB and PNB form cannot be conducting [3].

Organic–inorganic nanocomposites with an organized structure has been extensively studied because they combine the advantages of the inorganic materials (mechanical strength, electrical and magnetic properties, and thermal stability) and the organic polymers (flexibility, dielectric, ductility, and processibility), which are difficult to obtain from individual components [4]. To obtain materials with syncretistic advantage between PANI and inorganic nanoparticles (NPs), various composites of PANI with inorganic naonoparticles such as Cu [5], tellurium [6], lithium [7], and TiO_2 [8] have been reported. Micrometer-sized manganese zinc ferrites particles have recently been reported with PANI by chemical oxidation of aniline [9]. Very recently, Mahyar et al. reported the degradation of C.I. Basic Violet 2 (BV2; New Fuchsin) by using TiO_2–SiO_2 NPs as photocatalyst synthesized by the sol-gel method [10]. Similar work has been reported such as, degradation of azo dyes by using synthesized NPs (ZnO, $CaAl_2O_4$, and $CaZnO_2$) as photocatalysts under natural sunlight [11–13].

In order to obtain materials with superior stability against the environment, we have synthesized PANI/ Zr-Co-substituted nickel ferrite composites. They were characterized by X-ray diffraction (XRD), UV–vis, and scanning electron microscopy (SEM), and were used as photocatalyst for the degradation of methylene blue (MB). The effects of nickel ferrite concentrations in the composite on photodegradation have also been investigated in the present work.

2. Experimental

2.1. Chemicals

The chemicals used for the synthesis of PANI and their composites with nanomaterial were Fe $(NO_3)_3.9H_2O$ (98%, Aldrich), $Co(NO_3)_2.6H_2O$ (96%, Harris Reagent), $NiCl_2.6H_2O$ (>99.5%, Merck), $ZrOCl_2.4H_2O$ (96%, BDH), ammonia solution (26%, Riedel Dehaen), aniline chloride (99%, Merck), ammoniumperoxy disulfate (97%, Merck), methanol (99.8%, Merck), and acetone (98%, Merck). These were used as such without further purification.

2.2. Preparation of Zr-Co-substituted nickel ferrite

Zr-Co-substituted nickel ferrite ($NiFe_{1.2}Zr_{0.4}$-$Co_{0.4}O_4$) nanomaterial was prepared by the chemical co-precipitation method. For this purpose, the stoichiometric molar solutions for different metal salts were prepared in the deionized water. Then all these solutions were mixed in a beaker and heated up to 60˚C with continuous vigorous stirring. Ammonia solution (2 M) was added drop wise under vigorous stirring until pH reached above 11.0. The mixture was stirred continuously for further 4 h to obtain the homogeneity in the samples. The brown color precipitates were obtained after addition of precipitating agent and were washed repeatedly with deionized water until the pH reduced to 7.0. The precipitates were dried in an oven at 100˚C and finally annealed at 850˚C in a box furnace (Vulcan, A550) for 8 h. The obtained powder was used for further analysis.

2.3. Preparation of PANI/ Zr-Co-substituted nickel ferrite composite

The 0.2 M aniline chloride solution was taken in a beaker and in this beaker weighed amount of Zr-Co-substituted nickel ferrite powder was added. After that 0.2 M ammonium peroxydisulphate was added in the solution mixture drop wise with continuous stirring for 4–6 h at temperature of 2–5˚C. Polymerization of aniline chloride was allowed to take place in the presence of fine graded Zr-Co-substituted nickel ferrite particles. The resulting precipitates were filtered and washed with acetone and finally with deionized water until the filtrate becomes colorless. Acetone is used to dissolve any unreacted aniline chloride. After washing, the precipitates were dried at 60–70˚C in an oven. The dried samples were grinded into a fine powder in agate mortar pestle. These materials were stored in desiccator and were used as photocatalyst for the degradation of MB.

2.4. Degradation of MB

In the photodegradation experiments, 40 mL of MB solution with the concentration of 10^{-5} mL^{-1} was prepared. Four samples containing 40 mL of MB and 0.2 g of each composite having different (%) age of Nps

12.5, 25, 37.5, and 50%, with 5%, 25%, 5%, and 50% wt were taken and the solutions poured into photo reactor. The UV lamp model Philips HPK 300 W was turned on and after every 30 min the dye solution was taken out and it was centrifuge at 2,000 rpm. The absorbance of the solution was measured at wavelength of 665 nm which is the λ_{max} of MB. The decolorization efficiency (%) has been calculated as:

$$\text{Efficiency} = \frac{c_i - c_r}{c_i} \times 100 \quad (1)$$

where c_i is the initial and c_r is the remaining concentration of the dye.

2.5. Characterization

The phase and purity of nickel ferrite was determined using powder XRD analysis by using BRUKER D8 focus X-ray diffractometer which uses Cu Kα as radiation source operated at 40 kV and 40 mA. The crystallite size of samples was estimated by Scherer's equation. The optical properties were performed by using UV–Visible/NIR spectrophotometer (Lambda 750 Shimadzu). The surface morphology of the synthesized composite was determined by using field emission SEM (HitachiS-4800 FESEM). The specific surface area and pore volume of the synthesized materials was determined by Brunauer–Emmett–Teller (BET) analysis (Micromeritics, tristar II 3020). The oxidation states of the elements were determined by using ESCALAB 250Xi X-ray photoelectron spectrometer (XPS) analysis. The UV irradiation was provided by a high-pressure mercury lamp (OSRAM 300 W).

3. Results and discussions

3.1. XRD

Fig. 1 show XRD patterns for PANI and PANI/Zr-Co-substituted nickel ferrite composites. XRD pattern of PANI suggests that it exhibits a semi-crystalline behavior. The broad peaks at $2\theta = 20.4$, 25.4, and 28.2° are the characteristic peaks for PANI as reported earlier [14]. The prominent peaks at $2\theta = 20.4$, 25.4, and 28.2° in XRD pattern of composite indicate the presence of PANI and the extra peaks at $2\theta = 35.83$, 37.20, 43.5, 50.1, 54.3, 57.2, 63.0, and 74.8° with miller indices 311, 222, 400, 331, 422, 511, 440, and 533, respectively, match with standard pattern (ICDD-00-003-0875) which confirms that these peaks are related to the substituted nickel ferrite. The presence of peaks for both the materials i.e. PANI and Zr-Co-substituted nickel ferrite confirms the formation of composite.

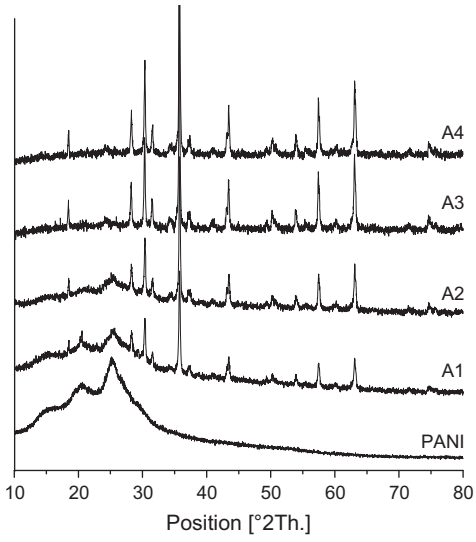

Fig. 1. XRD patterns for PANI and its composites (PANI) = PANI, (A1) = 12.5% $NiFe_{1.2}Zr_{0.4}Co_{0.4}O_4$, (A2) = 25% $NiFe_{1.2}Zr_{0.4}Co_{0.4}O_4$, (A3) = 37.5% $NiFe_{1.2}Zr_{0.4}Co_{0.4}O_4$, and (A4) = 50% $NiFe_{1.2}Zr_{0.4}Co_{0.4}O_4$.

It is also observed that with the increase in concentration of NPs in composite, the intensity of NPs peaks increases while that of PANI decreases. The crystalline size of the substituted nickel ferrite has been calculated by using well-known Scherer's formula which is found to be 43 nm. The values of lattice constant and cell volume are also calculated and are found in the range of 8.363Å and 584.91 Å^3, respectively. The values of lattice constant and cell volume are slightly higher than the standard values which is due to higher atomic radii of substituents i.e. Co^{2+} (0.74Å) and Zr^{4+} (0.80 Å) than that of Fe^{3+} (0.64 Å).

3.2. UV/Visible spectroscopy

The UV/Visible spectra for PANI and its composites are shown in Fig. 2. It is clear from the figure that two distinct peaks appeared at 373 and 417 nm which correspond to exciton absorption of the quinoid ring and the π–π^* transition of the benzenoid ring, respectively. These results are in agreement with already reported in the literature [15,16]. The peaks' intensity slightly decreases with an increase in nickel ferrite NPs in the PANI which is due to the decrease in PANI concentration. The band gap for PANI is calculated by Tauc Plot and is found to be 2.2 eV which is in agreement with that of reported earlier [17]. The value of band gap increases from 2.2 to 2.4 eV with an increase in NPs contents which is due to the slightly shift in peaks to lower wavelength [18].

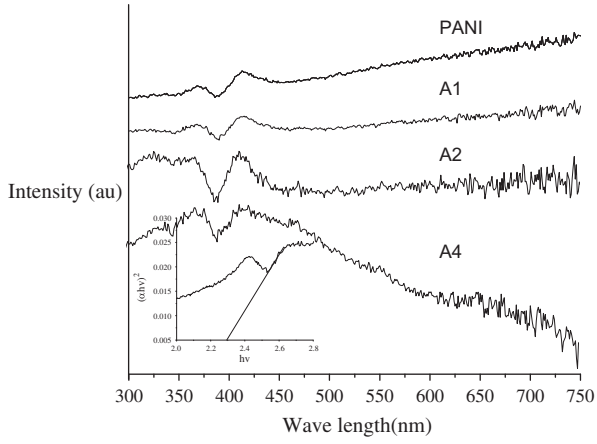

Fig. 2. UV/Visible spectra for PANI and its composites.

3.3. Scanning electron microscopy

The surface morphology and particles size was investigated by SEM analysis. Scanning electron micrographs of pure PANI, substituted nickel ferrite, and their composites are shown in Fig. 3((a)–(e)). SEM image of pure PANI shows the formation of smooth sheet and their surface is plane (Fig. 3(a)). The NPs are round shaped (Fig. 3(b)) and the particle size is found in the range of 40–50 nm. Some of the particles agglomerate into larger particles. The SEM images for the composites are shown in Fig. 3((c)–(e)) which shows that the NPs are decorated on the surface of PANI. The surface of the composite is porous and porosity increase with the increase in NPs in the composite which is beneficial for the adsorption of MB and its degradation.

3.4. BET studies

The BET study has been used to investigate the surface area and pores volume for the PANI and the substituted nickel ferrite/PANI composites. The parameters such as BET and Langmuir surface area and pore volume are shown in Table 1. It is clear from the table that the surface area and pore volume increase with the increase in substituted ferrite content. The increase in surface area and pore volume suggests that composite materials are more beneficial for the photodegradation as compared to PANI.

3.5. XPS study

The XPS analysis was carried out to determine oxidation states of the elements present in the synthesized materials. The XPS survey for PANI and its composite with Zr-Co-substituted nickel ferrite (50% content) is shown in Fig. 4. The XPS analysis indicates that the all the peaks are related to the elements present in the synthesized material which confirm that there is no other elemental impurity. The peak at 532 eV corresponds to the adsorbed oxygen [19] while the peak at around 400 eV corresponds to N1s indicating the trivalent oxidation state of nitrogen.

The XPS spectra for Ni2p, Zr3d, Co2p, Fe2p, and C1s are shown in Fig. 5(a)–(e), respectively. The Ni2p spectrum shows two peaks at around 855 and 862 eV in Fig. 5(a) that correspond to the signals from Ni 2p3/2 and Ni2p1/2, respectively, in the divalent oxidation state. The Zr3d spectra (Fig. 5(b)) consist of two peaks with binding energies around 182 and 184 eV which correspond to the signal from Zr3d3/2 and Zr3d5/2, respectively, which are in the tetravalent oxidation state. The peaks appeared at 781 and 796 eV correspond to Co2p3/2 and Co2p1/2, respectively, and revealing the divalent oxidation state of cobalt (Fig. 5(c)). The peak appears at around 711 and 725 eV (Fig. 5(d)) indicates the existence of Fe2p3/2 and Fe2p1/2, respectively, with trivalent oxidation state. The C1s spectrum is shown in Fig. 5(e); a peak appeared at 285 eV which correspond to the carbon in the aniline. The surface composition of the composite has also been investigated by the XPS analysis and the results are given in Table 2. It is clear from Table 2 that all the elements are in agreement with the composite composition.

3.6. Degradation of MB

3.6.1. Influence of reaction time

Residence time in light is one of the most important parameter that affects the photo-degradation of MB. The relationship between degradation and reaction time is shown in Fig. 6. It is clear from figure that the degradation of MB increases with the increase in reaction. It was also observed that the degradation was very rapid during the initial stage of the reaction and after 30 min it began to slow down. The ultimate degradation was found beyond 97% during the investigated reaction time of 150 min.

When PANI and its composites were illuminated with UV light, it absorbs photons to generate electron–hole pairs. These electrons and hole react with water molecules to generate hydroxyl radicals ($OH^{\cdot}$). The rate of degradation relates to the formation of OH radical which is the critical species in the degradation process. The equilibrium adsorption of reactants on the catalyst surface and the rate of reaction of OH radicals with other chemicals plays significant role in the rate of degradation [20].

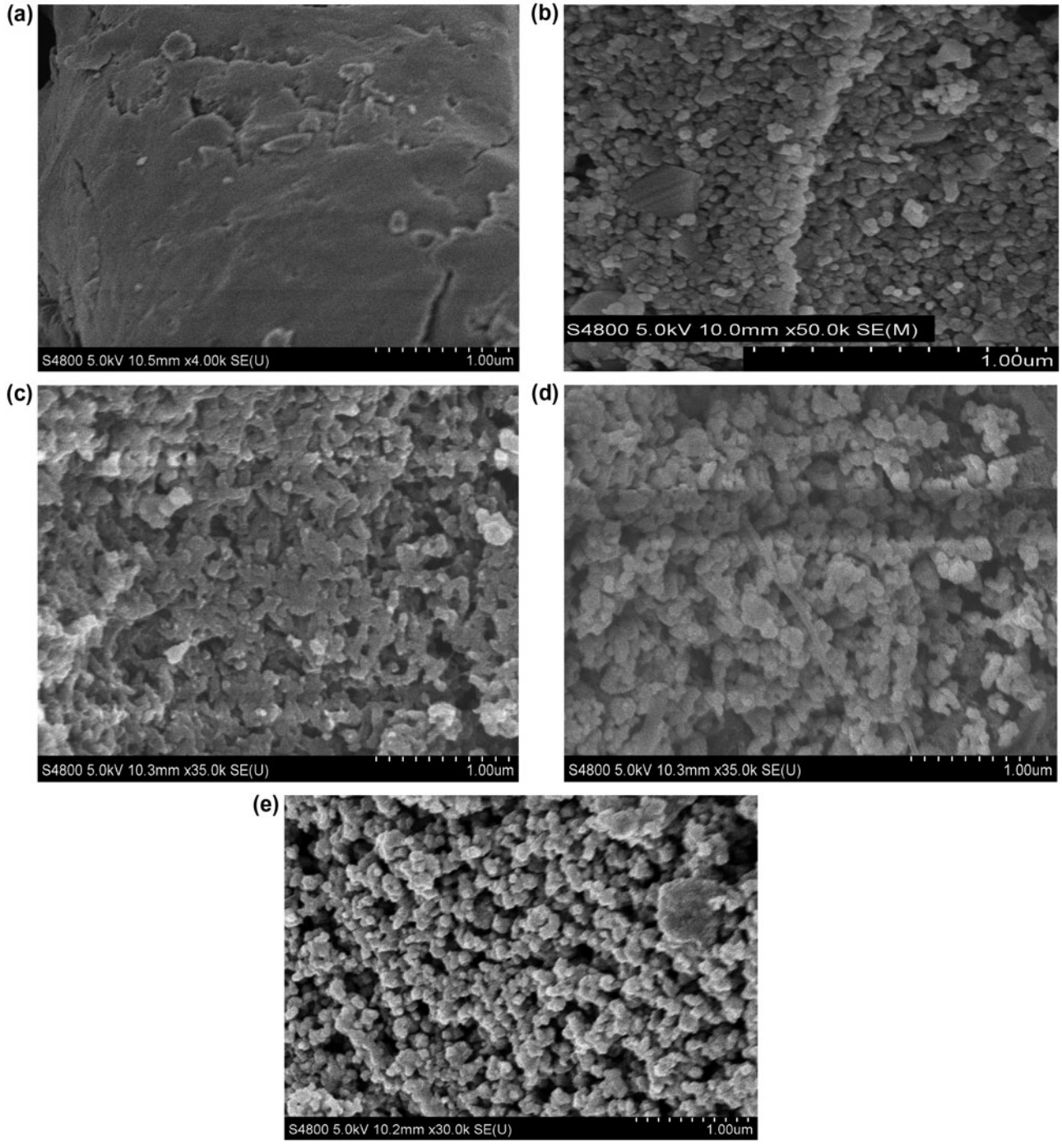

Fig. 3. SEM images for (a) = PANI, (b) = $NiFe_{1.2}Zr_{0.4}Co_{0.4}O_4$ NPs, (c) = 12.5% $NiFe_{1.2}Zr_{0.4}Co_{0.4}O_4$, (d) = 37.5% $NiFe_{1.2}Zr_{0.4}Co_{0.4}O_4$, and (e) = 50% $NiFe_{1.2}Zr_{0.4}Co_{0.4}O_4$.

The surface of PANI/NPs composite is porous as shown in SEM image and BET analysis (Table 1). These pores act as active sites to adsorb the MB molecule. These adsorbed molecules of MB could easily captured by photogenerated oxidizing species $OH^{\cdot}$ and degraded immediately, resulting a rapid degradation of MB in first 30 min. As the time precede, availability of these active sites decreased and also oxidizing species (OH) which results in decrease in rate of degradation of MB.

Table 1
BET and Langmuir Surface area and maximum pore size of substituted PANI and nickel ferrite/PANI composites

Samples	BET surface area (m^2/g)	Langmuir surface area (m^2/g)	Maximum pore volume (cm^3/g)
PANI	6.8971	11.2720	0.002854
A1	14.2641	37.3429	0.004377
A2	34.2377	53.8788	0.004871
A4	53.4599	91.9178	0.005172

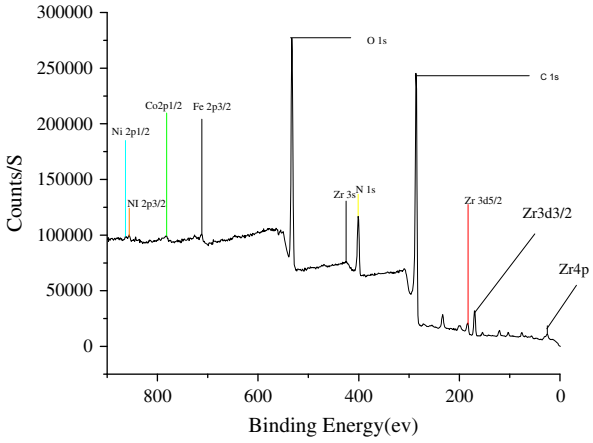

Fig. 4. XPS survey for PANI composite with 50% $NiFe_{1.2}Zr_{0.4}Co_{0.4}O_4$.

3.6.2. Effect of nanomatrial (%) age in composite

The effect of Cr-Co-substituted nickel ferrite NPs concentration into the composite was also examined. The increase in Nps concentration from 12.5%, 25%, 37.5% to 50% wt in composite increases the degradation rate. It is important to mention that bubbles were observed during the experiments. These bubbles are expected because of O_2 produced from photolysis by composite and CO_2 produced from complete degradation of MB. The generation of bubbles increased with an increase of the Nps (%) age in composite. The increase in the rate of degradation is due to the fact that as the ferrite content increase in the composite, the surface area as well as the pore volume increase (Table 1) which is responsible for the increase in the photodegradation rate of MB.

In photodegradation reaction, electron excited from valence band to the conduction band and leaving hole, this hole reacts with water molecules to generate $OH^{\cdot}$. With the increase in NPs (%) age in composite, the light penetration through the solution also increased and more $OH^{\cdot}$ was generated. The SEM images and BET analysis reveal that the surface of the catalyst becomes more porous which increase the adsorption of MB and as a result the degradation increases.

Table 2
The amount of element (atomic%) for Zr-Co-substituted nickel ferrite/PANI composites investigated from XPS analysis

S. No	Element	Atomic (%)
1	Zr	4.839
2	C	85.564
3	Fe	4.865
4	Co	2.098
5	Ni	2.634

The maximum photodegradation was observed in case of 50% content of nanomaterials into the composite.

The percentage degradation of MB which is 97% for the composite having 50% nickel ferrite content is compared with the other photocatalysts reported in literature. It is clear from Table 3 that percentage degradation in the present work is much higher as compared to other photocatalysts which suggest that the present materials (PANI/Zr-Co-substituted nickel ferrite composite) with 50% content can be efficiently used for the degradation of MB.

3.6.3. Photocatalytic degradation kinetics

Data are fitted to first- and second-order kinetic model to investigate the mechanism for the degradation of MB. The first-order equation is given as:

$$\log(q_e - q_t) = \log q_e - \frac{k_1}{2.303}t \quad (2)$$

where q_e and q_t are amount of MB degrade at equilibrium and time "t", respectively, and k_1 is the specific rate constant for first-order reaction [28]. A plot of log ($q_e - q_t$) vs. t for first-order kinetic is shown in Fig. 7(a). The value of specific rate constant increases from 9.6×10^{-3} to 17×10^{-3} s^{-1} (shown in Table 4) with the increase of NPs (%) age which is due to increase in the porosity of the surface and surface area of material (as indicated by SEM and BET results) which act as active sites and increase the adsorption of MB. As a

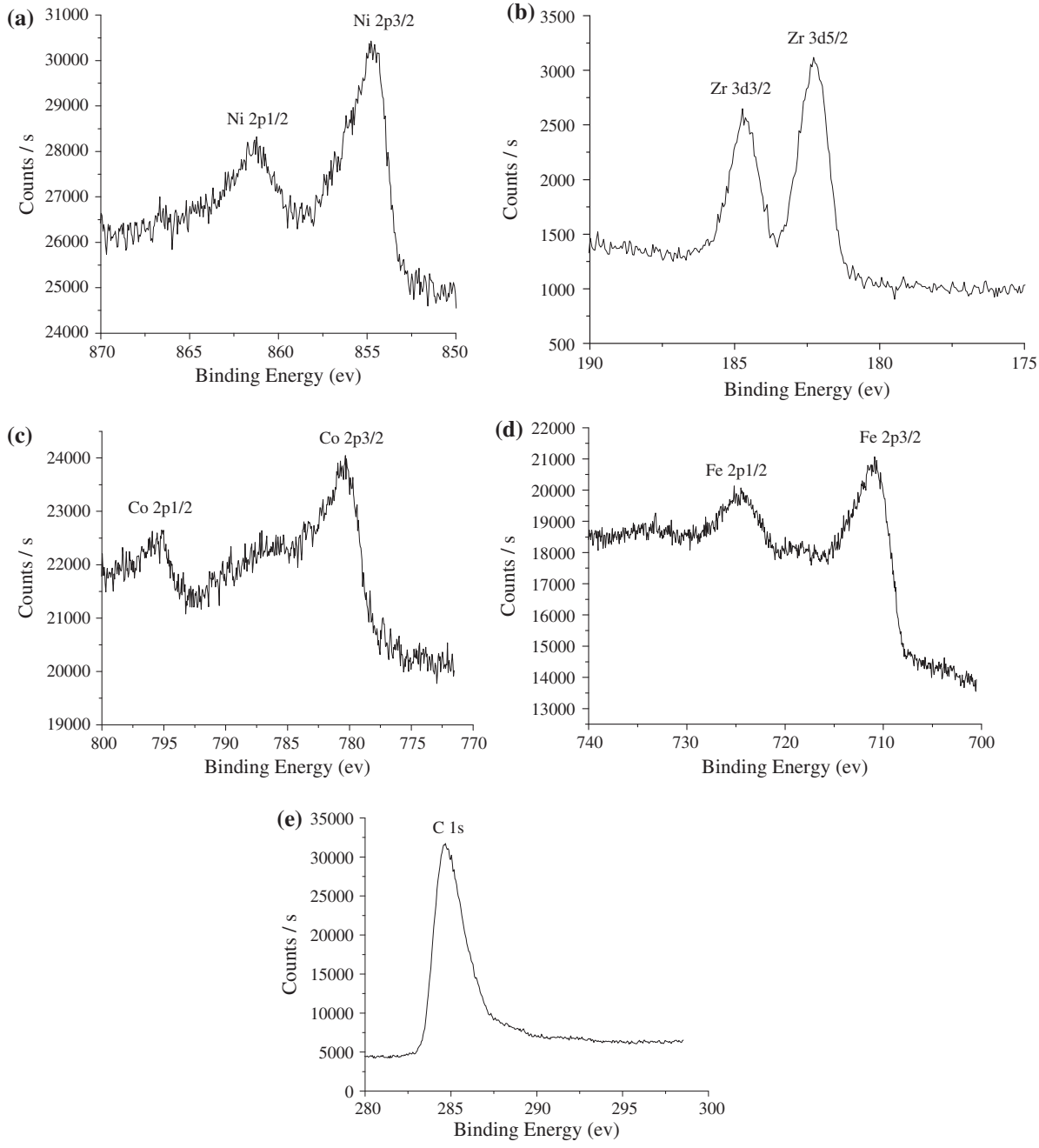

Fig. 5. XPS spectra for (a) Ni2p, (b) Zr3d, (c) Co2p, (d) Fe2p, and (e) C1s.

result, the degradation as well as the specific rate constant increase. The linear regression correlation coefficients (R^2) varied in the range of 0.9358–0.9947.

The second-order equation is given as:

$$\frac{t}{q_t} = \frac{1}{k_2 q_e^2} + \frac{1}{q_e} t \tag{3}$$

The graph has been plotted between t/q_t vs. t (shown in Fig. 7(b)) and the value of q_e and k_2 are calculated from the slope and intercept, respectively and their values are given in Table 4. Linear regression correlation coefficients (R^2) value calculated from plot of t/q_t vs. t for second-order kinetic model that ranges from 0.7396 to 0.9556 indicate that experimental data does not obey second-order kinetic model. From above

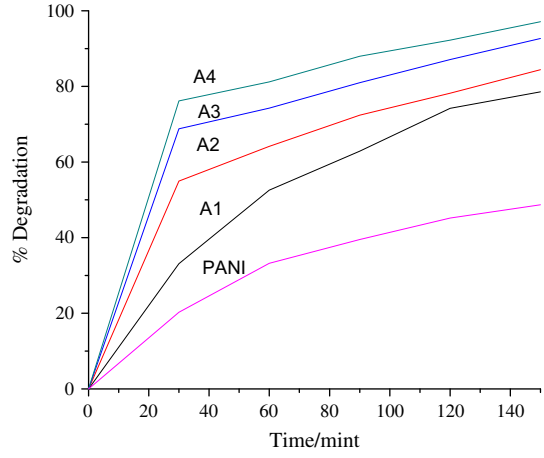

Fig. 6. Influence of time of the photodegradation of MB.

discussion, it can be suggested that rate of degradation of MB follows first-order kinetic.

The rate of degradation of MB increases with the increase of NPs (%) age in PANI/NPs composite as shown in Table 4 as indicated by value of first-order specific rate constant. The controlling factor of this oxidation reaction is the concentration of NPs which produce $OH^{\cdot}$ radical during course of reaction. The proposed mechanism is:

$$\text{PANI/NPs Composite} + h\nu \rightarrow e^{-}_{cb} + h\nu^{+}_{vb} \quad (4)$$

$$h\nu^{+}_{vb} + OH^{-} \rightarrow {}^{\cdot}OH \quad (5)$$

$$H^{+} + e^{-}_{cb} \rightarrow H^{\cdot} \quad (6)$$

$$O_2 + e^{-}_{cb} \rightarrow O^{\cdot}_2 \xrightarrow{H^{\cdot}} HO^{-}_2 \quad (7)$$

$$HO^{-}_2 + h\nu^{+}_{vb} \rightarrow HO^{\cdot}_2 \quad (8)$$

Table 4
First-order specific rate constant for k_1, second-order specific rate constant k_2, and correlation coefficient R^2

	First order		Second order	
Sample	k_1 (sec^{-1})	R^2	k_2 (L^{-1} mol sec^{-1})	R^2
PANI	0.0077	0.9815	0.0605	0.8677
A1	0.0096	0.9914	0.3799	0.7396
A2	0.0087	0.9947	0.055	0.9556
A3	0.0120	0.9626	0.0726	0.9293
A4	0.0170	0.9358	0.1535	0.8508

$$\text{Dye} + OH^{\cdot} \rightarrow \text{Degradation Product} \quad (9)$$

PANI/NPs composite involved in oxidation-reduction process becomes excited by UV-light as it activates the composite surface by exciting an electron from valence band to the conduction band and leaving hole. This electron and hole reacts individually with water molecules to generate $OH^{\cdot}$.

OH^{-} and H^{+} are involved in the photodegradation reaction traps h^{+}_{vb} and e^{-}_{cb} and make them available for the reactions taking place at the surface of PANI/NPs and prevent the recombination of e^{-}_{cb} and h^{+}_{vb}. Hydroxyl radicals attack is assumed to be the primary mechanism for photo oxidation as suggested by Turchi and Ollis [29]. And holes are likely to react with OH^{-} because it is readily absorbed to the catalyst surface.

By summing it up, in degradation process, light energy was adequately absorbed by NPs present in PANI/NPs composite; therefore, composite having high percentage of NPs produces large amount of $OH^{\cdot}$ radical groups rapidly and oxidation reaction proceed very quickly.

Table 3
Comparison of investigated photocatalyst with other reported in literature

S. No.	Catalyst	Degradation (%)	References
1.	PANI	28.00	[21]
2.	PANI/ZnO	79.00	[21]
3.	TiO_2 (nano-tube arrays)	53.00	[22]
4.	N + S co-doped TiO_2	66.00	[22]
5.	N-doped TiO_2	67.00	[23]
6.	TON-3	70.00	[24]
7.	TON-2	92.00	[24]
8.	PANI/TiO_2 (1:500)	81.74	[25]
9.	P25	82.00	[26]
10.	(PANI-$NiFe_2O_4$)	88.13	[27]
11.	PANI/Nickel ferrite	97.00	Present work

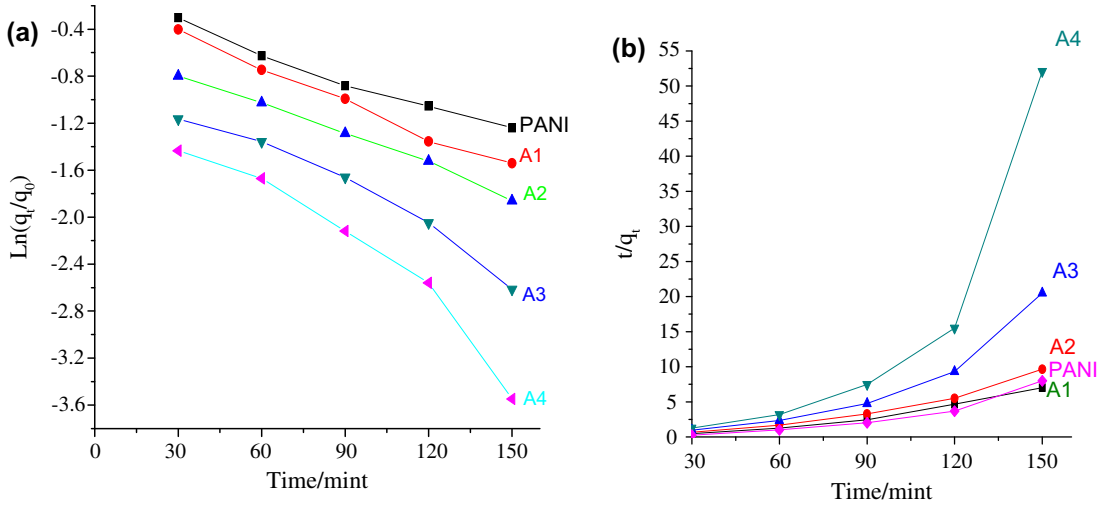

Fig. 7. (a) first-order kinetic plot and (b) second-order kinetic plot for the photodegradation of MB.

4. Conclusion

The PANI/Zr-Co-substituted nickel ferrite composite was synthesized by adding nanomaterials during polymerization reaction of aniline chloride by ammonium peroxydisulphate. The XRD confirmed the formation of polymer/NPs composites. SEM images indicate that nanoparticals decorate the surface of PANI which is in the form of sheets and increase the porosity on the surface of PANI which act as active sites for the adsorption and degradation of MB. The BET analysis confirmed that the surface area increases with the increase in ferrite content in the composite. The XPS studies confirmed the oxidation state of different elements in the composite and NPs. The kinetics studies showed that the degradation process follow the first-order kinetic model. The photodegradation of MB increases with the increase in nanoparticle content in the composite and maximum 97% degradation is observed for the sample with 50% ferrite nanoparticle composite which is much higher as compared to other photocatalyst reported in the literature. The high degradation percentage by present composite indicates that this can be used as photocatalyst for the removal of MB from water.

Acknowledgment

One of the authors (M.N. Ashiq) is highly thankful to Bahauddin Zakariya University, Multan for the financial support for this project.

References

[1] S.F.B. Tahir, N. Rahmili, I. Izzuddin, M. Salleh, M. Yahaya, A.A. Umar, M.H. Jumali, Effect of ZnO addition on structural properties of ZnO-PANI/carbon black thin films, Sains Malaysiana. 41 (2012) 1001–1004.
[2] B.B. Vhanakhande, K.V. Madhalea, V.R. Puri, Microwave properties of electropolymerised polyaniline thin films on stainless steel, Arch. Phys. Res. 4 (2013) 54–60.
[3] A.H. Elsayed, M.S. Mohy Eldin, A.M. Elsyed, A.H. Abo Elazm, E.M. Younes, H.A. Motaweh, Synthesis and properties of polyaniline/ferrites nanocomposites, Int. J. Electrochem. Sci. 6 (2011) 206–221.
[4] J.B. Bhaiswar, M.Y. Salunkhe, S.P. Dongre, Synthesis, characterization, thermal stability and D.C. electrical conductivity of PANI/Pbs nanocomposite, Int. J. Comput. Mater. 3 (2013) 115–121.
[5] V. Ali, R. Kaur, N. Kamal, S. Singh, S.C. Jain, H.P.S. Kang, M. Zulfequar, M. Husain, Use of Cu^{+1} dopant and it's doping effects on polyaniline conducting system in water and tetrahydrofuran, J. Phys. Chem. Solids 67 (2006) 659–664.
[6] S. Kazim, V. Ali, M. Zulfequar, M. Mazharul Haq, M. Husain, Electrical, thermal and spectroscopic studies of Te doped polyaniline, Curr. Appl Phys. 7 (2007) 68–75.
[7] K.S. Ryu, B.W. Moon, J. Joo, S.H. Chang, Characterization of highly conducting lithium salt doped polyaniline films prepared from polymer solution, Polymer 42 (2001) 9355–9360.
[8] J. Xu, W. Liu, H.L. Li, Titanium dioxide doped polyaniline, Mater. Sci. Eng. C 25 (2005) 444–447.
[9] H. Nguyen-Cong, V.D.G. Guadarrama, J.L. Gautier, P. Chartier, Oxygen reduction on $NixCo_{3-x}O_4$ spinel particles/polypyrrole composite electrodes: Hydrogen peroxiden formation, Electrochem. Acta 48 (2003) 2389–2395.

[10] A. Mahyar, M.A. Behnajady, N. Modirshahla, Characterization and photocatalytic activity of SiO_2–TiO_2 mixed oxide nanoparticles prepared by the sol-gel method, Indian J. Chem. 49 (2010) 1593–1600.
[11] N. Madhusudhana, K. Yogendra, K.M. Mahadevan, S. Naik, H. Gopalappa, Photocatalytic degradation of coralene dark red 2B dye using calcium aluminate ($CaAl_2O_4$) catalyst, J. Environ. Sci. Indian J. 6 (2011) 1–5.
[12] N. Madhusudhana, K. Yogendra, K.M. Mahadevan, S. Naik, Photocatalytic degradation of Coralene Dark Red 2B azo dye using calcium zincate nanoparticle in presence of natural sunlight, an aid to environmental remediation, Int. J. Chem. Eng. Appl. 2 (2011) 301–305.
[13] K. Yogendra, K.M. Mahadevan, S. Naik, N. Madhusudhana, A comparative study of photocatalytic activities of two different synthesized ZnO composites against Coralene Red F3BS dye in presence of natural solar light, Int. J. Environ. Sci. Res. 1 (2011) 11–15.
[14] S. Khasim, S.C. Ragghavendra, M. Revanasiddeappan, K.C. Sajjan, M. Lakshmi, M. Faisal, Synthesis, characterization and magnetic properties of polyaniline/γ-Fe_2O_3 composites, Bull. Mater. Sci. 34 (2011) 1557–1561.
[15] A. Ubul, R. Jamal, A. Rahman, T. Awut, I. Nurulla, T. Abdiryim, Solid-state synthesis and characterization of polyaniline/multi-walled carbon nanotubes composite, Synth. Met. 161 (2011) 2097–2102.
[16] U.M. Casado, M.I. Aranguren, N.E. Marcovich, Preparation and characterization of conductive nanostructured particles based on polyaniline and cellulose nanofibers, Ultrason. Sonochem. 21 (2014) 1641–1648.
[17] H.S. Abdulla, A.I. Abbo, Optical and electrical properties of thin films of polyaniline and polypytole, Int. J. Electrochem. Sci. 7 (2012) 10666–10678.
[18] S.N. Dolia, R. Sharma, M.P. Sharma, N.S. Saxena, Synthesis, X-ray diffraction and optical band gap study of nanopartical of $NiFe_2O_4$, Indian J. Pure Appl. Phys. 44 (2006) 774–776.
[19] C. Basavaraja, W.J. Kim, P.X. Thinh, D.S. Huh, Charge transport properties of polyaniline-gold/graphite oxide composite films, Bull. Korean Chem. Soc. 33 (2012) 449–452.
[20] B.Z. Lin, X.L. Li, B.H. Xu, Y.L. Chen, B.F. Gao, X.R. Fan, Improved photocatalytic activity of anatase TiO_2-pillared $HTaWO_6$ for degradation of methylene blue, Mesoporous Microporous Mater. 155 (2012) 16–23.
[21] V. Eskizeybek, F. Sari, H. Gulce, A. Gulce, A. Avci, Preparation of the new polyaniline/ZnO nanocomposite and its photocatalytic activity for degradation of methylene blue and malachite green dyes under UV and natural sun lights irradiations, Appl. Catal., B 119–120 (2012) 197–206.
[22] G. Yan, M. Zhang, J. Hou, J. Yang, Photoelectrochemical and photocatalytic properties of N+S co-doped TiO_2 nanotube array films under visible light irradiation, Mater. Chem. Phys. 129 (2011) 553–557.
[23] Y. Ku, W. Chen, W. Hou, Photocatalytic decomposition of Methylene Blue with nitrogendoped TiO_2 under visible light irradiation, Sustainable Environ. Res. 23 (2013) 15–21.
[24] G. Yang, Z. Jiang, H. Shi, T. Xiao, Z. Yan, Preparation of highly visible-light active N-doped TiO_2 photocatalyst, J. Mater. Chem. 20 (2010) 5301–5309.
[25] F. Wang, S. Min, Y. Han, L. Feng, Visible-light-induced photocatalytic degradation of methylene blue with polyaniline-sensitized TiO_2 composite photocatalysts, Superlattices Microstruct. 48 (2010) 170–180.
[26] R. Rahimi, M. Rabbani, S.S. Moghaddam, Application of N, S-codoped TiO_2 photocatalyst for degradation of methylene blue, Mater. Chem. Phys. 116 (2009) 376–382.
[27] M.R. Patil, V.S. Shrivastava, Photocatalytic degradation of carcinogenic methylene blue dye by using polyaniline-nickel ferrite nano-composite, Der Chemica Sinica. 5 (2014) 8–17.
[28] L.V. Jian-xiao, C. Ying, X. Guo-hong, Z. Ling-yun, W. Su-fen, Decoloration of methylene blue simulated wastewater using a UV-H_2O_2 combined system, J. Water Reuse Desalin. 1 (2011) 45–51.
[29] C.S. Turchi, D.F. Ollis, Mixed reactant photocatalysis: Intermediates and mutual rate inhibition, J. Catal. 119 (1989) 483–496.